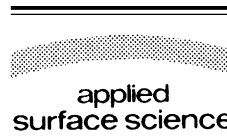




ELSEVIER

Applied Surface Science 188 (2002) 306–318



www.elsevier.com/locate/apsusc

Quantitative modelling in scanning force microscopy on insulators

Adam S. Foster^{a,*}, Alexander L. Shluger^b, Risto M. Nieminen^a

^aLaboratory of Physics, Helsinki University of Technology, P.O. Box 1100, FIN-02015 Hut, Finland

^bDepartment of Physics and Astronomy, University College London, Gower Street, London WC1E 6BT, UK

Received 2 September 2001; accepted 25 September 2001

Abstract

We analyse the mechanisms of contrast formation in non-contact atomic force microscopy (NC-AFM) on insulators and use comparisons of theoretical models with experiment to establish tip and surface properties. The results for the CaF₂ (1 1 1) surface provide information about the character of the tip–surface interaction, tip sharpness and electrostatic potential, and the distance range of imaging. We analyse whether knowledge of the electrostatic potential at the imaging distance is enough to interpret the image and show that account of the surface deformation is crucial for quantitative understanding of the image contrast. Then we turn to a more complex CaCO₃ (1 0 1 4) surface, which has a complex anion. We demonstrate that with an ionic tip the atomic structure of the CO₃²⁻ group cannot be resolved, and we also study the dependence of imaging on the tip orientation. Again, the surface deformation induced by the tip during scanning plays a crucial role in image contrast. We argue that if the relation between the tip structures, potential and observed image could be uniquely established for some systems, these systems could serve as a reference for tip characterisation in further studies. © 2002 Elsevier Science B.V. All rights reserved.

Keywords: AFM; Insulators; Surfaces; Modelling; Structure; Tip–surface interaction

1. Introduction

Non-contact atomic force microscopy (NC-AFM) is now able to study a wide range of surface properties at the atomic scale including surface topography, measurements of adhesion and the strength of individual chemical bonds, magnetic properties and molecular manipulation (see, for example [1,2] and more recent publications [3–7]). Sophisticated theoretical approaches have proved to be an essential ingredient in any progress made, and detailed analysis of the NC-AFM operation performed in several groups

(see, for example [8–15]) led to further optimisation of experiments and qualitative understanding of the origins of image contrast. Although it is by now fairly common that experimentally studied systems are simulated by advanced theoretical methods [6,16–23], image interpretation is still very complex. Improvements in analysis have allowed, however, the relation between modelling and experiment to enter a new stage where quantitative comparison between the two provides image interpretation. Nevertheless, the number of systems where atomic resolution has been obtained experimentally and where the chemical identity of the surface features has been unambiguously established remains limited to the Si(1 1 1) 7 × 7 [3,4], CaF₂ (1 1 1) [6,24], graphite [21] and xenon [22] surfaces. The chemical identity of atomic features observed on surfaces of other binary compounds, such as

* Corresponding author. Tel.: +358-9-451-3103;
fax: +358-9-451-3116.
E-mail address: asf@fyslab.hut.fi (A.S. Foster).

NaCl, KBr, NiO, TiO₂, InAs and Al₂O₃, remains unclear, mainly due to the uncertainty in the structure and chemical composition of tips used in these experiments.

Chemical resolution of different species at surfaces of these and more complex compounds remains among the main challenges for NC-AFM. Many of these systems have ionic or mixed ionic-covalent bonding where the electrostatic component of the interaction within the sample and with the tip is very significant. In this case, the result depends qualitatively on the sign and the spatial distribution of the electrostatic potential produced by the whole tip. In spite of “non-contact” type of imaging, tip-induced surface deformation in many cases determines the details of image pattern, providing crucial clues for interpretation [6,25]. Both of these factors are difficult to directly establish experimentally. However, as has been demonstrated in recent publications, quantitative comparison between modelling and experiment can be used as a tool for extracting the tip–surface interaction (see, for example [26–28]) and gaining information about the tip and surface structure [24,29]. Moreover, if the relation between the tip structure, potential and observed image could be uniquely established for some systems, these systems could serve as a reference for tip characterisation in further studies.

A detailed analysis of systems already imaged successfully suggests that: (i) in most cases tips are covered by the surface material; (ii) in imaging Si(1 1 1), the image contrast is determined by the onset of the chemical bond formation between silicon atoms on the tip and at the surface; (iii) the electrostatic interaction between the tip and surface ions plays the most important role in contrast formation on ionic surfaces; (iv) the tip and surface deformation during imaging plays an important role in contrast formation; (v) exchange of tip and surface species caused by the interaction-induced instabilities are common features of many experiments.

In this paper, we develop this approach further by considering imaging of the CaF₂ (1 1 1) and CaCO₃ (1 0 1 4) surfaces. The method of calculation is presented in Section 2. In Section 3 we analyse the results of our theoretical modelling of the NC-AFM imaging of the CaF₂ (1 1 1) surface. In Section 3 we present new results for the imaging of the CaCO₃ (1 0 1 4) surface and summarise our conclusions in Section 4.

2. Method of calculations

The model used in this study is the same as that described in [24,25,30,31]. Hence, in this section we will only summarise the main features and focus in detail only on those aspects of modelling that are specific to this study. A schematic diagram of the tip and surface setup used in the calculations is shown in Fig. 1. We assume a conducting tip having a conical shape on the macroscopic scale with a sphere of radius r at the end. As in our previous studies, the tip is terminated by an oxide cluster in the form of a 64-atom MgO cube embedded into the macroscopic tip to represent a generic oxide ‘nano-tip’. The cube is orientated so that it is symmetric about the z -axis with either a single oxygen or magnesium ion at the lowest point of the tip.

The tip–surface interaction in our model includes three main components: (i) the microscopic chemical force between the tip atoms and the surface, including the van der Waals force between ions; (ii) the macroscopic van der Waals force between the tip apex and the surface; (iii) the electrostatic force due to work functions, charging and polarisation of conducting materials [32,33]. Their relative contributions depend on the specific tip–surface combination studied. To integrate macroscopic and microscopic interactions in the same model we used the approach described in [24,25,30,31].

The distance dependence of the van der Waals force is calculated using the method described in [34]. A Hamaker constant was estimated to be equal to 1.0 eV using the data found in [34]. We note that this is an average number, which is characteristic of the interaction between semiconductor and insulator. Its more precise determination is difficult. It enters the expressions for the van der Waals force in a product with the effective tip radius, which is in most cases unknown. Therefore, instead of varying both parameters, in our further analysis we tried to estimate only the tip radius.

The microscopic force is calculated using a periodic static atomistic simulation technique and the MARVIN2 code [35]. The empirical parameters used for the tip, CaF₂ surface and tip–surface interactions are the same as in [36]. The calcite surface parameters are from [37] and the remaining tip–surface interaction parameters are taken from [38]. They reproduce the structural properties of bulk calcite and give excellent

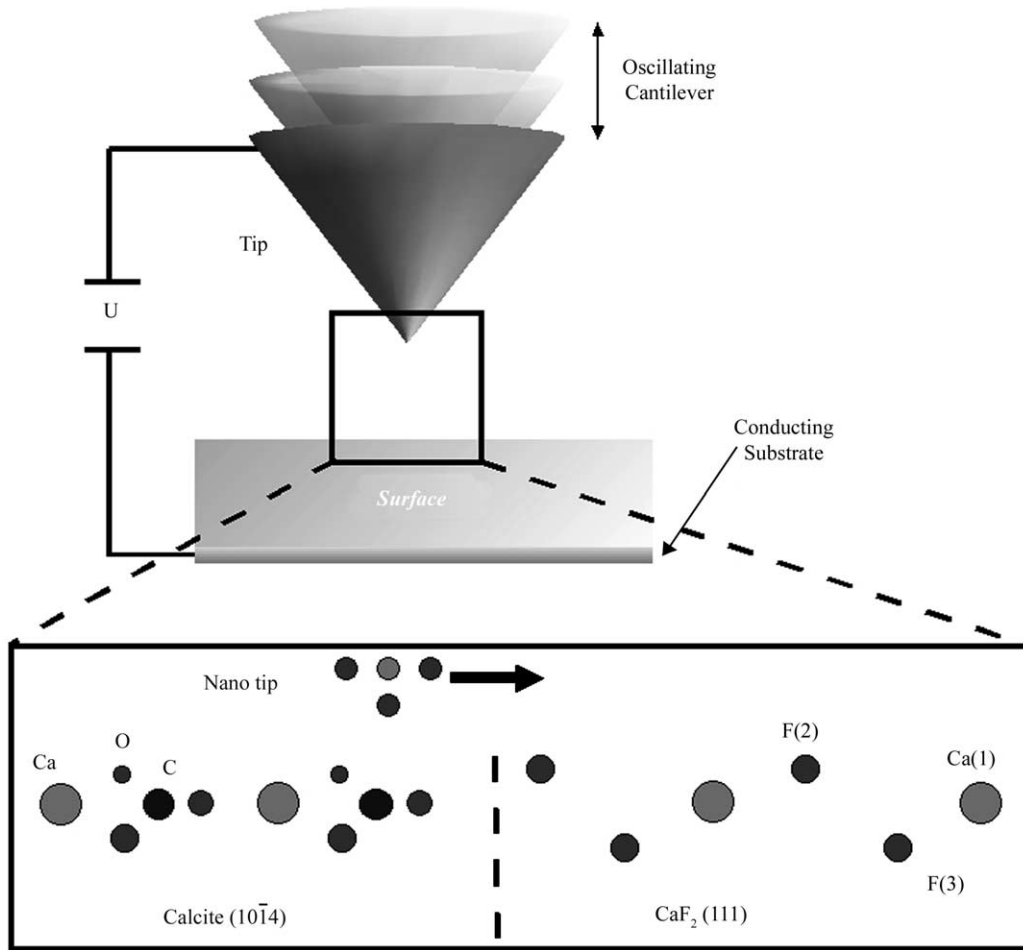


Fig. 1. Schematic view of the tip-surface model used to simulate scanning and the two specific surfaces, the calcite (1 0 1 4) surface and the CaF_2 (1 1 1) surface, considered as examples in this study.

agreement with *ab initio* calculations. The unit cell used in the simulations to represent the CaF_2 surface is equivalent to extending the single layer shown in Fig. 1 by $4 \times 8 \times 3$, and for calcite it is equivalent to extension by $4 \times 3 \times 3$. The bottom of the nano-tip and the top of the surface (top two layers) are relaxed explicitly in the same way as in previous studies [24,36]. The tip is virtually scanned across the surface at range of tip-surface separations to generate a force grid, $F(x, y, z)$.

The next stage of the modelling is to calculate the oscillations of the cantilever under the influence of this tip-surface force. The oscillations of the cantilever over a surface point (x, y) driven by an external force in

a force field $\mathbf{F}(z)$ are described by the equations of motion discussed in detail in [30]. Any interaction of the tip with the surface will cause a detuning of the resonance frequency f_0 to become f as the tip oscillations are maintained at constant amplitude. In this paper, we assume that any damping is completely compensated by an external force and that $\mathbf{F}(z)$ does not depend on time. A more general analysis of the cantilever dynamics and dissipation could be found, for example, in [10,11,15,39–41].

The experimental images and scanlines can be produced via the ‘constant frequency detuning, Δf ’, or ‘constant-height’ mode of dynamic mode SFM operation. Therefore, simulated images are calculated in the

same manner with an interpolation of the calculated detuning for a given tip–surface separation generating the image. All calculated force curves and scanlines were produced assuming a cantilever amplitude of 35 nm for CaF₂, and 67 nm for calcite, a resonance frequency of 77 kHz and a spring constant of 6 N/m, as in the main experimental results discussed.

3. Results

3.1. CaF₂ (1 1 1) surface

In spite of the significant number of studies on ionic insulators and binary semiconductors, the CaF₂ (1 1 1) surface so far remains the only binary ionic system where the chemical identity of atomically resolved surface features has been unambiguously established [6,24]. In this section we will briefly summarise the theoretical analysis of the experimental data in order to highlight the important steps and results. We will then consider whether a simpler analysis based on the calculation of the electrostatic potential at the shortest tip–surface distance could provide the same interpretation of the experimental data.

3.1.1. Long-range interactions

The average resonance frequency detuning during imaging (of the order of 10–100 Hz) is determined primarily by the background force, whereas image contrast results from small variations (~ 0.1 –1 Hz) of detuning due to the short-range chemical interaction between the tip and the surface. The main contributions [42] to the background force are long-range electrostatic forces due to residual surface charges, image forces and long-range van der Waals forces depending on the tip composition, radius and shape. It is now a fairly common practice to measure frequency detuning vs. distance curves, $\Delta f(d)$, before and after imaging surface topography [4,5,24]. These measurements can be used to characterise the effective tip radius, chemical composition, and the tip and surface charging [24,29], and even to extract the purely short-range interaction [27]. In the case of site-specific $\Delta f(d)$ measurements this opens an exciting possibility to probe directly the chemical interactions, and ultimately single bond formation between the tip and surface atoms [5].

The results obtained for the CaF₂ (1 1 1) and other ionic surfaces demonstrate the following characteristic features:

- i) It has been common practice to minimise the long-range electrostatic interactions by applying bias voltage similar to that described in [24,26,31]. The compensating bias voltage exhibits strong variations from one cleave to another (from -10 to $+4$ V in [24]) and even small variations when probing different locations on the surface. The precise effect of voltage is not well understood. Partly it equilibrates the contact potential between tip and sample holder, and partly compensates for the electrostatic force due to the surface charging after cleavage via a capacitance force.
- ii) For further analysis one needs to align theoretical and experimental curves using a common origin. Based on the results of theoretical modelling [29,30], at short distances, perturbations in the tip–surface interaction due to tip contamination by surface ions may lead to instabilities in cantilever oscillations. If these instabilities are not observed experimentally, it can be assumed that the tip does not reach a critical distance from the surface, which in many calculations is predicted to be of the order of 4 Å.
- iii) The measured force curves strongly depend on the tip preparation. Using the SFM model described above, one can fit theoretical curves to experimental data obtained at different oscillation amplitudes for different tip radii. Free parameters of the fit in this case are the tip radius and the bias voltage. If only electrostatic and van der Waals forces are involved, the fitted parameters are quite unique and a similar fit could not be found with an increased bias and reduced radius. This is due to the very different behaviour of van der Waals and electrostatic forces as a function of distance [29]. If the tip and/or surface are charged, this is clearly reflected in the long-range behaviour of the $\Delta f(d)$ curves.

3.1.2. Interpretation of NC-AFM images of the CaF₂ (1 1 1) surface

The tip parameters found in the way described above were used as input values for calculating the

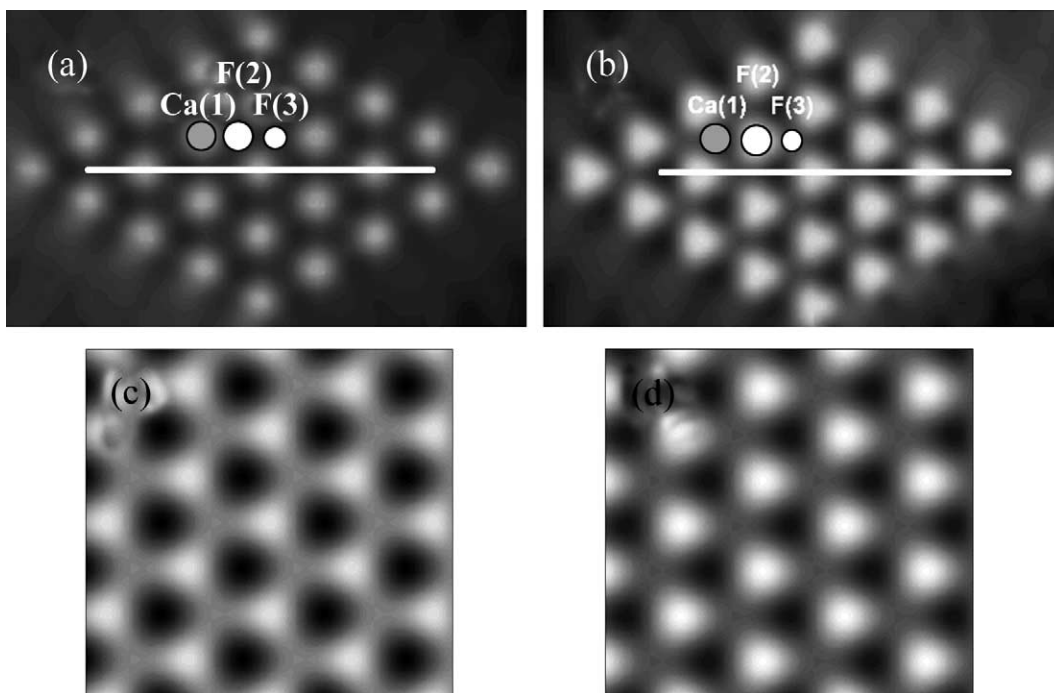


Fig. 2. Simulated images of the CaF_2 (1 1 1) surface at a height of 4.0 \AA using (a) a negative potential tip and (b) a positive potential tip. Electrostatic potentials (in the range -10 to $+10 \text{ eV}$) of the CaF_2 (1 1 1) surface calculated with ab initio method, plotted with (c) positive potential as bright and (d) negative potential as bright.

background forces and aligning the absolute values for the frequency detuning of theory and experiment with each other in modelling NC-AFM images of the CaF_2 (1 1 1) surface in [6,24,36]. Both experiment and theory demonstrated that the contrast in images depends crucially on the nature of the tip. Modelling predicted that an anion-terminated tip with a negative potential would image the Ca^{2+} sublattice as bright and that the pattern of contrast would be rather disk-like at all tip–surface separations (see Fig. 2a). For a cation terminated tip with a positive potential, modelling predicted that the protruding F^- sublattice would be imaged as bright, producing a triangular pattern of contrast in images shown in Fig. 2b due to the interaction with the deeper F^- sublattice. The latter agrees with experiment, and is supported by the quantitative comparison of the experimental and theoretical scanlines calculated in the range of shortest tip–surface approach of $4.0\text{--}4.5 \text{ \AA}$. The characteristic triangular pattern is due to the formation of the secondary peaks or shoulders in the scanlines. Theory predicts that these shoulders should appear at 2.2 \AA from the main

peaks and this agrees well with the experimental average position of $2.3 \pm 0.4 \text{ \AA}$. Moreover, both theory and experiment predict that the relative height of the primary and secondary maxima decreases as the tip moves closer.

This overall agreement yields convincing evidence that in the experiments yielding the triangular pattern the tip had a positive potential and that the protruding F^- sublattice with the deeper F^- sublattice (see Figs. 2 and 3) was imaged as bright. On the other hand, in the images yielding the disk-like pattern the Ca ions were imaged as bright with a tip having a negative potential. Hence, the qualitative character of the CaF_2 image contrast pattern reveals the sign of the tip potential. Most tips used in NC-AFM imaging on insulators are initially oxidised. Having a positive or negative tip potential is equally probable, since during tip preparation and also during the experiment, the tip can easily be contaminated by picking up species from the surface. Unknown atomistic structure at the end of the tip usually prevents quantitative interpretation of SFM images. However, this problem could be overcome by

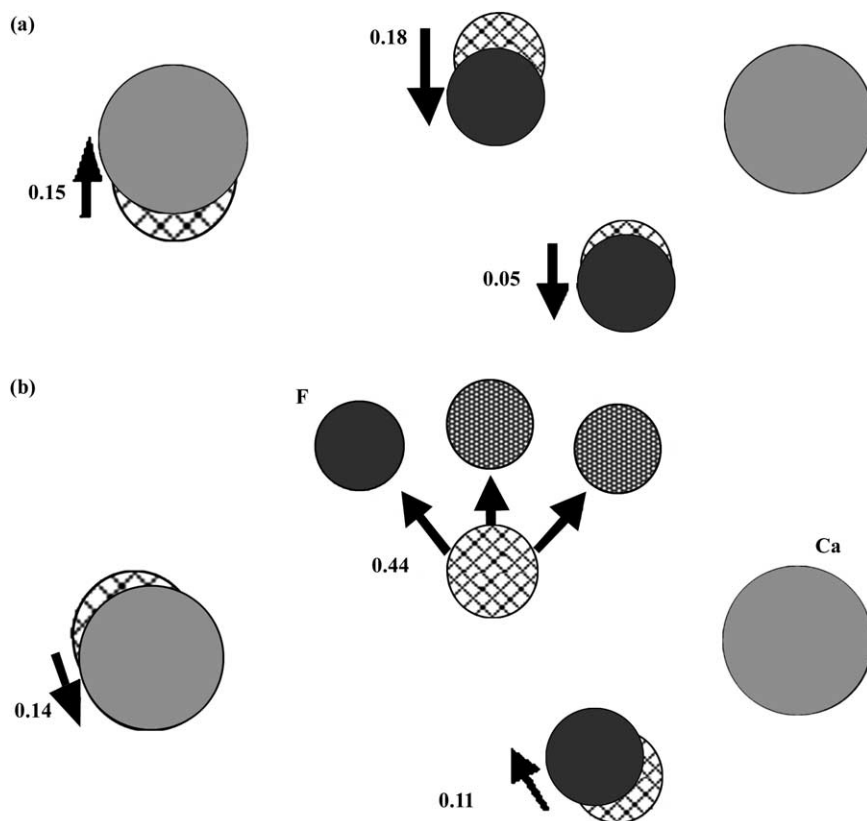


Fig. 3. Schematic diagram of atomic displacements of the CaF_2 (1 1 1) surface as the tip scans across at 0.4 \AA . The numbers are in \AA , and show the displacements when the tip is directly over that atom. The hatched atoms show the undisplaced position of the atoms when the tip is not in proximity, and the arrows give an indication of the displacement direction as the tip approaches. (a) Scanning with a negative potential tip. (b) Scanning with a positive potential tip. Note that the high F^- ion is displaced almost to the same height each time the tip approaches the surface in the vicinity of that ion.

using the CaF_2 (1 1 1) and other well-characterised surfaces for testing the sign of tip potential before and after scanning another sample.

3.1.3. Role of the surface electrostatic potential and relaxation in image contrast

The theoretical and experimental results obtained for the CaF_2 (1 1 1) surface provide a direct link between image pattern, tip potential and the distance range of the closest tip approach. This information can be used for testing other ideas. In particular, it has been demonstrated [11,27] that frequency detuning in NC-AFM is proportional to the surface potential at the distance of the closest tip approach. Assuming a point-charge tip and a rigid surface, this could provide

a simplified model, which could serve as a basis for much easier interpretation of NC-AFM images.

To test this possibility, in Fig. 2c we show the ab initio electrostatic potential of the static CaF_2 (1 1 1) surface at 4.0 \AA (Fig. 1 shows the atomic structure of the surface) with positive potential as bright and Fig. 2d shows the same potential with negative potential as bright. Both potentials demonstrate a triangular contrast pattern with brightest contrast over the Ca^{2+} ions in the positive image and over the protruding F^- ions in the negative image. This triangular pattern is due to the effect of the deeper layer of F^- ions on the interaction, but the important thing to note is that the contrast pattern is effectively identical and would be indistinguishable in an experiment. This is in direct

contradiction with the experiment and theoretical calculations discussed above, which demonstrate a disk-like pattern above Ca ions.

We believe that this discrepancy arises because simulations of scanning include the displacements of ions due to tip proximity, unlike the static surface seen in the electrostatic potential described above. Fig. 3a shows the displacements of the three sublattices in the CaF_2 (1 1 1) surface as a negative potential tip scans across them at 4.0 Å, and Fig. 3b shows the same for a positive potential tip. For a negative potential tip, the displacements are quite simple, with the F^- ions being pushed into the surface and the Ca^{2+} being pulled out. However, the displacement of the Ca ion towards the tip greatly increases the interaction between them, and any other interactions are almost insignificant. This domination of the interaction by the Ca causes the disk-like contrast seen in simulated images. The atomic displacements for a positive potential tip are more complex, but have less effect on the 'ideal' electrostatic picture. The Ca^{2+} ion is now pushed into the surface, and both the F^- ions are pulled out of the surface. The protruding F^- ion is actually pulled from the surface even before the tip is directly over the ion. However, since both the F^- ions are displaced out from the surface, both their interactions increase and the influence of the deeper F^- ion can still be seen in images, i.e. the triangular contrast pattern seen in the electrostatic potential is retained. This difference in the contrast pattern can be, and has been [6,24,36], used to directly interpret the contrast seen in experiments.

These results suggest that, although the map of the rigid surface electrostatic potential contains some information about the surface image, it cannot be used for reliable interpretation of experimental images. They emphasise the importance of the tip atomic structure (not just a point charge) and surface relaxation during scanning. As pointed out above, as the number of well-understood surfaces will grow, some of them may serve as a reference for checking the tip structure. These should be well-defined stable surfaces, which would be easy to cleave and prepare. Therefore, we have also studied the (1 0 1 4) surface of CaCO_3 , which is easy to cleave and which has a more complex surface structure. Previous attempts to image this and other similar minerals (see, for example [43–45]) did not resolve all chemical species.

3.2. CaCO_3 (1 0 1 4) surface

To establish an accurate picture of the physical and electronic structure of calcite, first ab initio calculations were performed using the plane wave basis VASP code [46,47], implementing density function theory (DFT), the generalised gradient approximation (GGA) of Perdew and Wang known as GGA-II [48], and ultra-soft Vanderbilt pseudopotentials [49,50] to represent the core electrons. The top two surface layers were allowed to relax fully, while the bottom layer was kept fixed to represent the bulk. The relaxation of the calcite surface was very small, with an inward relaxation of 0.1 Å by the outermost Ca ions being the largest displacement. The surface structure and the map of the electron density in Fig. 4 clearly demonstrate covalent bonding between the C and O atoms within CO_3 groups and the ionic character of the Ca species.

Fully simulating scanning of the calcite surface requires a large unit cell, which is far too demanding for ab initio techniques, hence empirical methods must be employed. A schematic diagram of the tip and surface setup used in the calculations is shown in Fig. 1. Fig. 5a shows a simulated 'constant-height' image at 4.25 Å produced using a negative potential tip, and Fig. 5b is produced with a positive potential tip at 4.25 Å. For a negative potential tip, the contrast is dominated by interaction over the Ca^{2+} ions (as shown by the dashed line). A positive potential tip at large tip–surface distance interacts with the negatively charged CO_3^{2-} group as a whole, however, at shorter distances it produces maximum brightness over the highest O atom in the carbonate group sticking out of the surface plane. As the orientation of carbonate groups along the surface axis alternates, this results in the zigzag line between contrast maxima shown in Fig. 5b, which can be characterised by a 13° angle between a given 'zigzag' and the vertical.

The complex displacements of atoms in the calcite surface play an important role in contrast formation and strongly amplify the image features described above. Scanning with a negative potential tip at 4.25 Å produces a combination of rotation/displacement of the carbonate group and displacement of the Ca ion (as shown in Fig. 6a). The Ca has a simple displacement out of the surface as the tip passes, but the carbonate group rotates as it is pushed into the surface. This combination

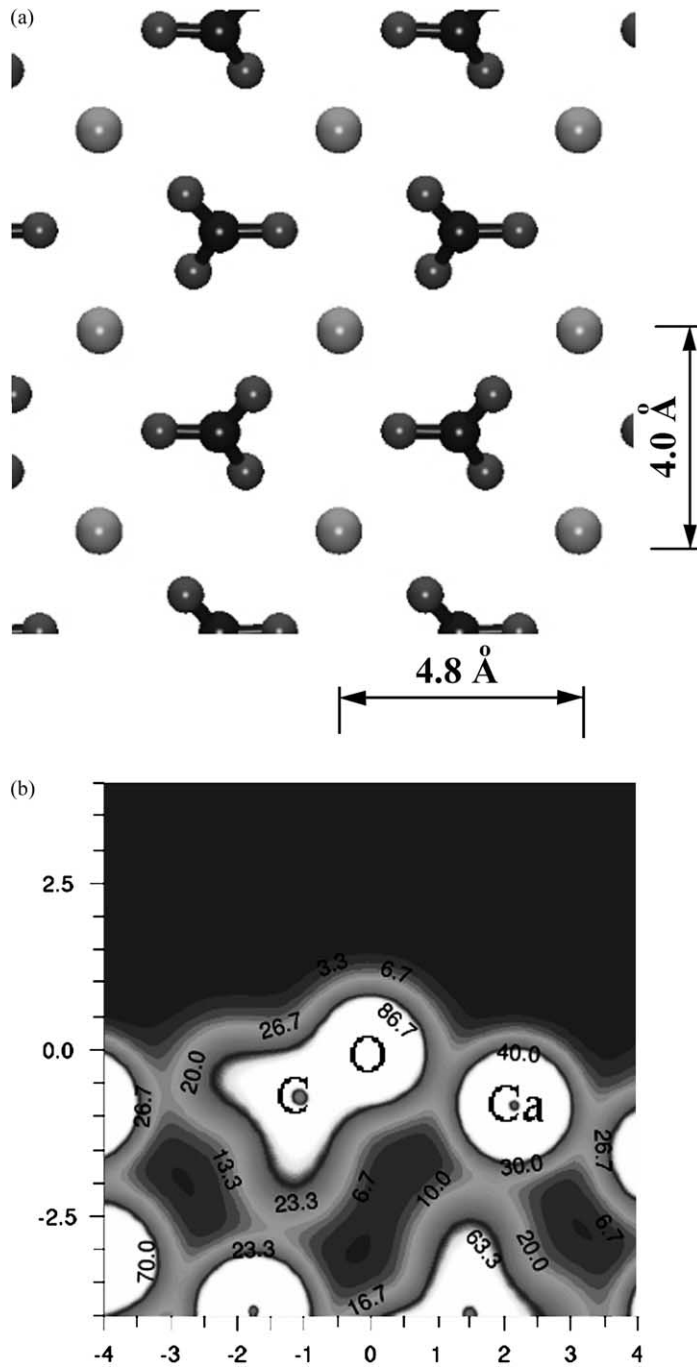


Fig. 4. (a) Top view of the calcite (1 0 1 4) surface. The atom colours are described in Fig. 1. (b) Side view of the ab initio charge density of the calcite surface. Note the strong covalent bond between C and O atoms in the carbonate group, and very small charge density between Ca and O. Distance is in Ångströms and charge density is in $0.1e \text{ \AA}^{-1}$.

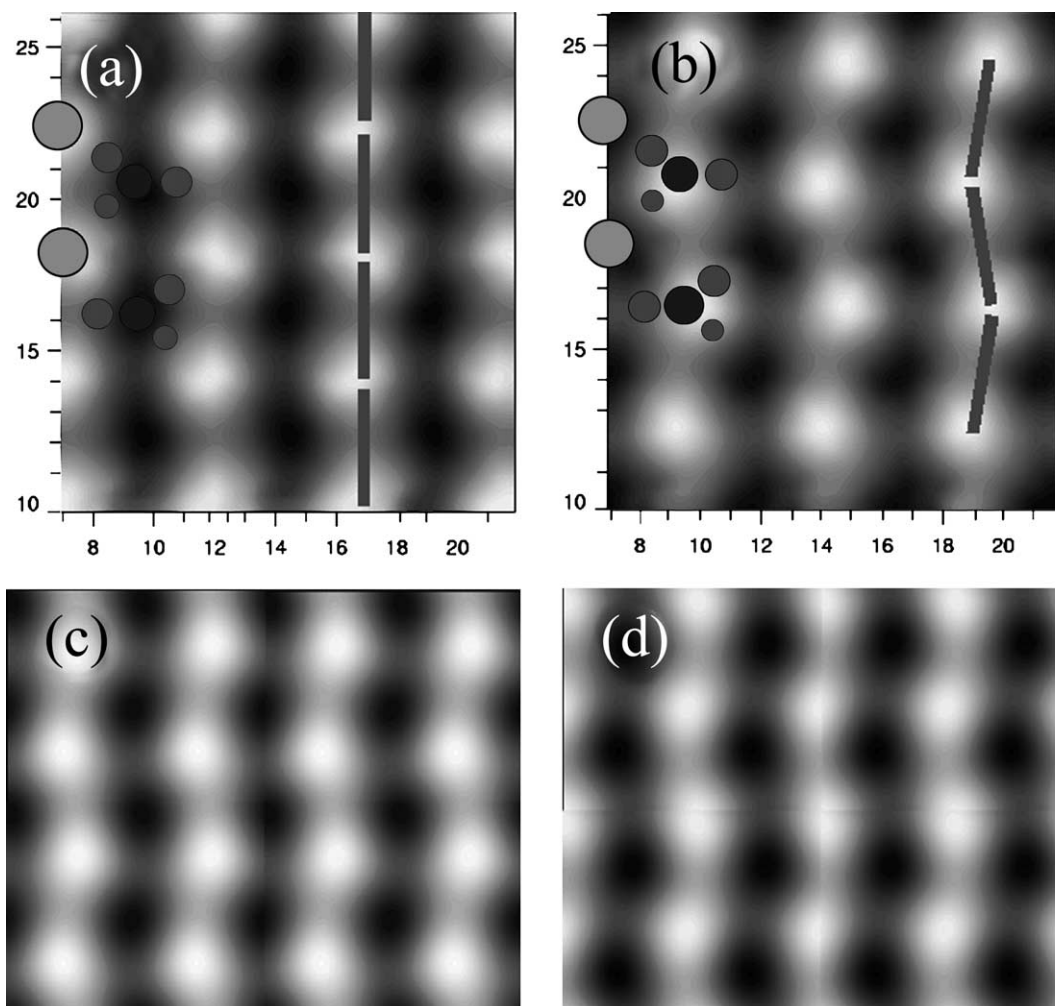


Fig. 5. Simulated images of the calcite (1014) surface at a height of 4.25 \AA using (a) a negative potential tip and (b) a positive potential tip. The disks show the positions of the Ca and carbonate group with similar colour scheme to Fig. 1, and the dashed line joins the points of maximum brightness in the images. Electrostatic potentials (in the range -10 to $+10 \text{ eV}$) of the calcite surface calculated with ab initio method, plotted with (c) positive potential as bright and (d) negative potential as bright.

reduces the influence of the orientation of the carbonate group on images, and the position of the Ca atom dominates contrast in images produced with a negative potential tip. For a positive tip (see Fig. 6b) the Ca atom is pushed into the surface, and the whole carbonate group is strongly displaced out with a slight rotation. The very large displacement of the highest oxygen of the carbonate (0.45 \AA) causes a very strong interaction with the tip, and its position dominates contrast in images with a positive potential tip. Again, this difference in contrast pattern can be used as a basis for

interpretation of experimental images. Fig. 6c shows the displacements of the calcite surface when scanning with a positive potential tip at 4.0 \AA . At this closer separation, the whole carbonate group at first displaces out from the surface considerably, and then actually flips up, pivoting on the middle oxygen atom. This kind of displacement causes extreme changes in the force, and is likely to prevent stable NC-AFM operation at these tip–surface distances.

It is interesting to see whether the image of the much more complex calcite surface could be characterised by

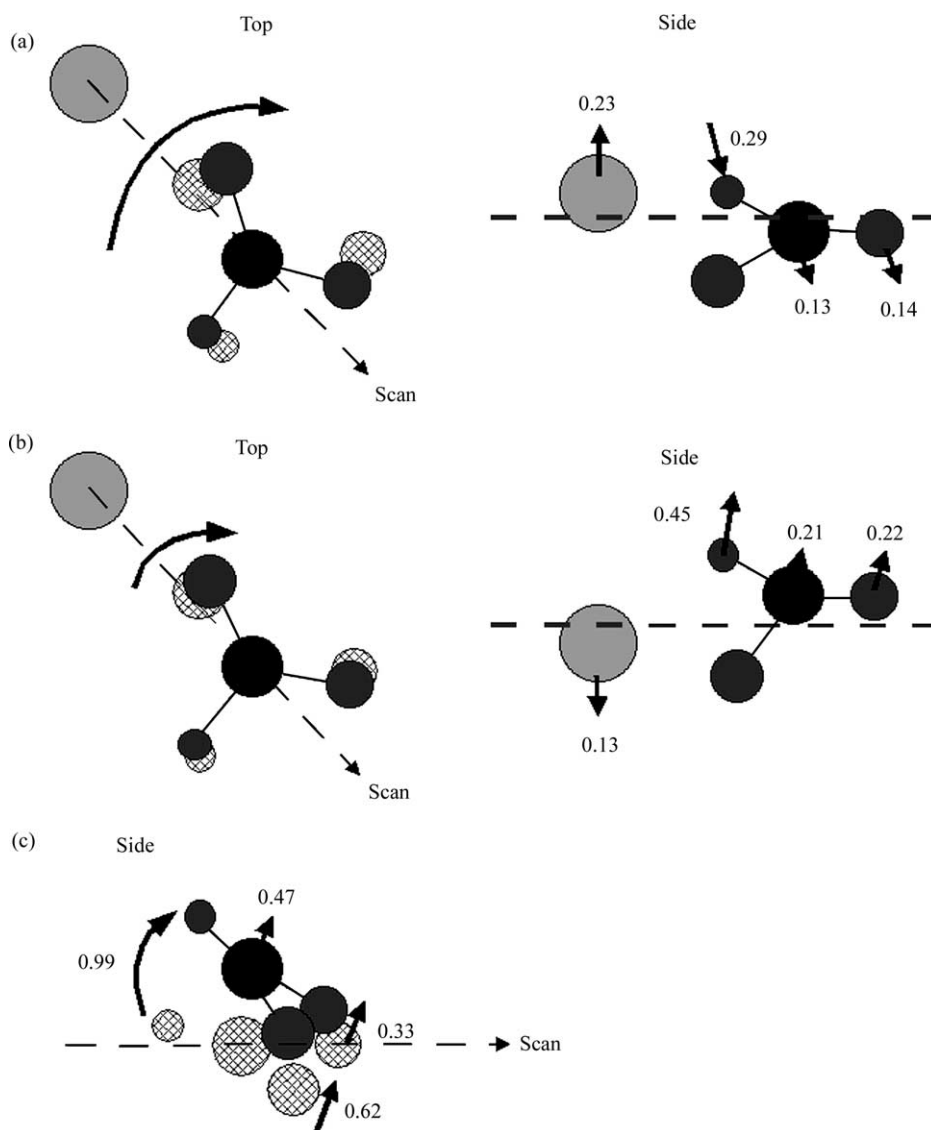


Fig. 6. Schematic diagrams of atomic displacements of the calcite (1 0 1 4) surface as the tip scans across at 4.25 Å. The numbers are in Ångströms, and show the displacements when the tip is directly over that atom. The atomic colour scheme is the same as in Fig. 1, and the size of the oxygen atoms in the carbonate group is in perspective, i.e. the larger the atom the further 'out' of the page it lies. The hatched atoms show the undisplaced position of the atoms when the tip is not in proximity, and the arrows give an indication of the displacement direction as the tip approaches. (a) Scanning with a negative potential tip. (b) Scanning with a positive potential tip. (c) Scanning at 4.0 Å from the surface with a positive potential tip causes the whole carbonate group to flip up from the surface.

its electrostatic potential. The strong covalent bonding between the carbon and oxygens in the carbonate groups (see Fig. 4b), contrasts strongly with the purely ionic picture seen in CaF_2 . Fig. 5c shows the ab initio electrostatic potential of the static calcite surface at

4.25 Å with positive potential as bright and Fig. 5d shows the same potential with negative potential as bright. Again we see that the contrast pattern is effectively identical with only superficial differences in the shape of contrast features. The contrast pattern

is made up of parallel rows of ellipsoids with their central axis alternating in direction down the rows. This is consistent with the alternating orientation of the carbonate groups on the surface (see Figs. 1 and 4). In the positive potential the ellipsoids are centred on the Ca^{2+} ions and in the negative potential they are centred on the carbonate group. There is no resolution of the individual elements of the carbonate groups in either potential, i.e. the C and O sublattices cannot be separated directly. However, the orientation of the ellipsoids does indicate the position of the highest

O atom and, hence, indirectly the position of the other elements of the carbonate group.

Another important issue concerns the effect of the tip structure on the image pattern. Although the tip used in these studies represents a highly idealised model, it can easily be modified to study the dependence of imaging on tip properties. The possibility of changing the sign of the tip potential has already been discussed, but it is also possible to study how the orientation of the tip affects imaging. Fig. 7a demonstrates how the tip–surface force as a function of

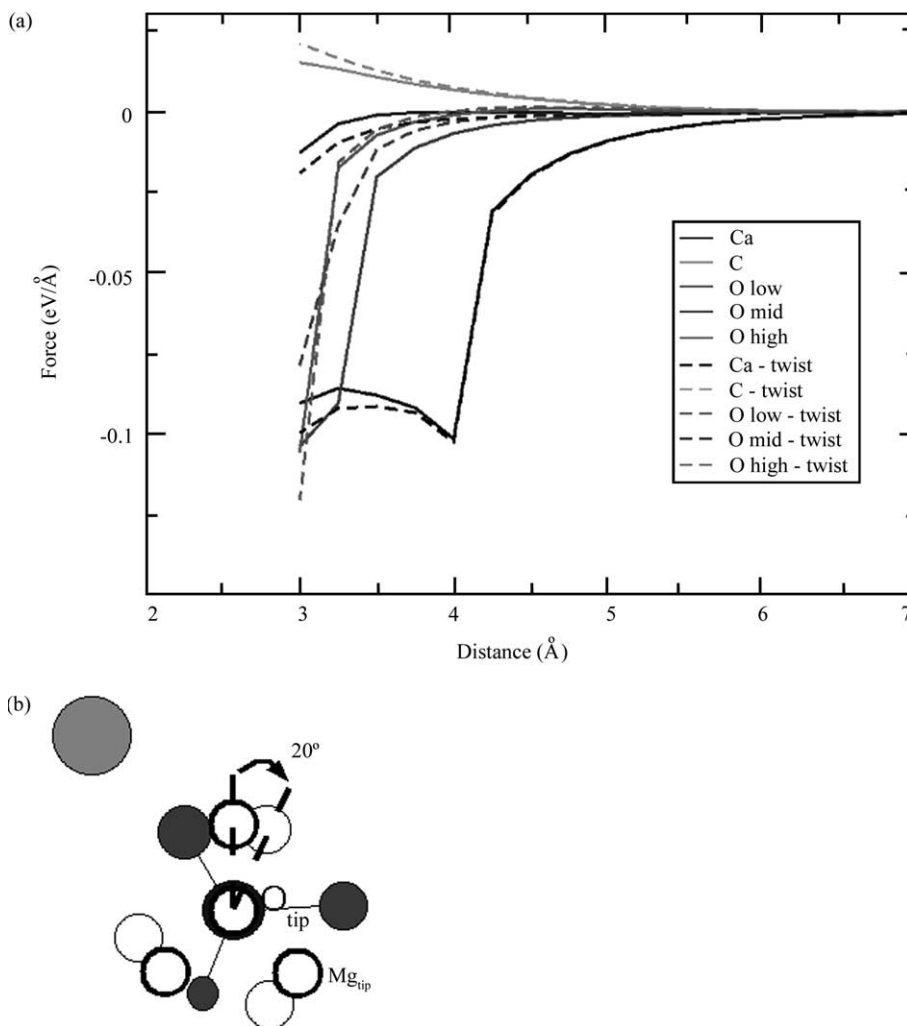


Fig. 7. (a) Comparison of the force as a function of tip–surface separation between a normal tip and a tip rotated by 20° around the z -axis. The curves are taken over the various sublattices in the calcite surface where curves marked with “twist” in the legend refer to the interaction of the rotated tip. (b) Schematic diagram showing how the orientation of the projection of the end of the MgO tip on the carbonate group changes when rotated.

distance changes when the MgO cube tip is rotated by 20° around the z -axis. As shown in Fig. 7b, this results in the rotation of the projection on the surface carbonate group of three Mg ions surrounding the O ions terminating the tip. Firstly, it is clear that the general characteristics remain the same, with the force curves keeping a similar shape. In fact, for the contrast dominating sites, such as the Ca atom, the force curve is identical until very close approach. Simulated images produced using this rotated tip are virtually indistinguishable from the original images shown above. However, clear differences in force curves can be seen when the tip is over the less ‘image significant’ ions, implying that the simplest changes in orientation of the tip can affect the tip–surface interaction.

4. Conclusions

We discussed the results of our recent modelling of NC-AFM imaging of surfaces of two relatively complex insulators—CaF₂ (1 1 1) and CaCO₃ (1 0 1 4). Good qualitative and even quantitative agreement between the theoretical and experimental data obtained using our theoretical model in previous studies [24,31] suggests that it captures correctly the main features of the tip–surface interaction. This gives us confidence in quantitative results of our calculations, such as the distance range of the shortest tip–surface approach during scanning and parameters of image corrugation. In particular, the results of this work and several previous studies suggest that the common shortest approach distance is about 3.0–4.5 Å, as measured between the unperturbed tip and the rigid surface.

The significant result of this work is, therefore, that at this distance range both the CaF₂ and CaCO₃ surfaces experience a very strong tip-induced deformation, which provides vital clues for image interpretation. The tip-induced surface deformation has been observed in our previous calculations on alkali halides and MgO [30,31], but it had a much smaller scale. This reflects the local surface “softness” as the displacements we observe are specific to particular ions (F[−]) or groups (CO₃^{2−}). These displacements decrease rapidly as the shortest tip–surface separation increases and images become similar to those given by the electrostatic potential (Figs. 2c and d and 5c and d).

By imaging at different distance one could therefore probe these surface properties.

We should also note that the CaCO₃ (1 0 1 4) surface provides the first example of a system with complex anion modelled for NC-AFM imaging. Our results suggest that with a relatively symmetric and simple oxide tip used in our calculations it should not be possible to resolve the carbon and oxygen species in the carbonate group. This results from the strong Coulomb interaction between this group and the tip, the tip-induced surface deformation and its displacement from the surface, and the discussed above convolution of the tip and carbonate group structures. The effects of convolution of the tip and surface features on atomic scale and tip-induced surface deformation are likely to be even more important for more complex surfaces. Our results suggest that these effects can be studied using site-selective force spectroscopy with low-temperature microscopes. We are currently looking into relation between the tip-induced local surface deformation and dissipation in NC-AFM imaging. To this end, a detailed analysis of the relation of the distance dependence of dissipation and surface deformation with surface phonons would be extremely useful.

Finally, we should note that, as the number of well-understood surfaces where NC-AFM images are reproducible and allow unique interpretation will increase, some of them could be used as reference systems for establishing the tip potential and nano-sharpness. If the reference and investigated sample could be mounted side by side as shown in Fig. 1 and imaged reproducibly one after another, this could offer possibilities for express-analysis and interpretation of images based just on a basic knowledge of their geometric and electronic structures.

Acknowledgements

We are grateful to EPSRC for financial support. ALS would like to acknowledge the support from the NATO grant CRG.974075. We are grateful to C. Barth and M. Reichling for extremely fruitful collaboration, which inspired this work and gave many good ideas, and to R. Bennowitz, E. Meyer, H. Hug and R. Hoffmann for very useful discussions and sharing with us their new results and ideas.

References

- [1] R. Bennewitz, C. Gerber, E. Meyer (Eds.), Proceedings of the NC-AFM'99, *Appl. Surf. Sci.* 157 (4) (2000).
- [2] U.D. Schwarz, H. Hölscher, R. Wiesendanger (Eds.), Proceedings of the NC-AFM2000, *Appl. Phys. A* 72 (2001).
- [3] F.J. Giessibl, S. Hembacher, H. Bielefeldt, J. Mannhart, *Science* 289 (2000) 422.
- [4] M.A. Lantz, H.J. Hug, P.J.A.v. Schendel, R. Hoffmann, A. Martin, A. Baratoff, A. Abdurixit, H.-J. Güntherodt, C. Gerber, *Phys. Rev. Lett.* 84 (2000) 2642.
- [5] M.A. Lantz, H.J. Hug, R. Hoffmann, P.J.A.v. Schendel, P. Kappenberger, S. Martin, A. Baratoff, H.-J. Güntherodt, *Science* 291 (2001) 2580.
- [6] A.S. Foster, C. Barth, A.L. Shluger, M. Reichling, *Phys. Rev. Lett.* 86 (2001) 2373.
- [7] P.M. Hoffmann, A. Oral, R.A. Grimble, H.O. Ozer, S. Jeffery, J.B. Pethica, *Proc. Roy. Soc. Lond. A* 457 (2009) (2001) 1161.
- [8] F.J. Giessibl, *Science* 267 (1995) 68.
- [9] F.J. Giessibl, *Phys. Rev. B* 56 (1997) 16010.
- [10] F.J. Giessibl, H. Bielefeldt, S. Hembacher, J. Mannhart, *Appl. Surf. Sci.* 140 (1999) 352.
- [11] U.D. Schwarz, H. Hölscher, R. Wiesendanger, *Phys. Rev. B* 62 (2000) 13089.
- [12] B. Gotsmann, C. Seidel, B. Anczykowski, H. Fuchs, *Phys. Rev. B* 60 (1999) 11051.
- [13] C. Loppacher, R. Bennewitz, O. Pfeiffer, M. Guggisberg, M. Bammerlin, S. Schar, V. Barwich, A. Baratoff, E. Meyer, *Phys. Rev. B* 62 (2000) 13674.
- [14] U. Dürig, *Appl. Phys. Lett.* 76 (2000) 1203.
- [15] U. Dürig, *New J. Phys.* 2 (2000) 1.
- [16] J. Tóbiš, I. Stich, R. Pérez, K. Terakura, *Phys. Rev. B* 60 (1999) 11639.
- [17] S.H. Ke, T. Uda, R. Pérez, I. Stich, K. Terakura 60 (1999) 11631.
- [18] A. Abdurixit, A. Baratoff, E. Meyer, *Appl. Surf. Sci.* 157 (2000) 355.
- [19] L.N. Kantorovich, A.L. Shluger, A.M. Stoneham, *Phys. Rev. Lett.* 85 (2000) 3846.
- [20] A.S. Foster, A.L. Shluger, *Surf. Sci.* 490 (2001) 211.
- [21] H. Hölscher, W. Allers, U.D. Schwarz, A. Schwarz, R. Wiesendanger, *Phys. Rev. B* 62 (2000) 6967.
- [22] H. Hölscher, W. Allers, U.D. Schwarz, A. Schwarz, R. Wiesendanger, *Appl. Phys. A* 72 (2001) S35.
- [23] K. Tagami, N. Sasaki, M. Tsukada, *Appl. Surf. Sci.* 172 (2001) 301.
- [24] C. Barth, A.S. Foster, M. Reichling, A.L. Shluger, *J. Phys.: Condens. Mat.* 13 (2001) 2061.
- [25] A.I. Livshits, A.L. Shluger, A.L. Rohl, *Appl. Surf. Sci.* 140 (1999) 327.
- [26] R. Bennewitz, M. Bammerlin, M. Guggisberg, C. Loppacher, A. Baratoff, E. Meyer, H.-J. Güntherodt, *Surf. Interf. Anal.* 27 (1999) 462.
- [27] M. Guggisberg, M. Bammerlin, C. Loppacher, O. Pfeiffer, A. Abdurixit, V. Barwich, R. Bennewitz, A. Baratoff, E. Meyer, H.-J. Güntherodt, *Phys. Rev. B* 61 (2000) 11151.
- [28] H. Hölscher, W. Allers, U.D. Schwarz, A. Schwarz, R. Wiesendanger, *Phys. Rev. Lett.* 83 (1999) 4780.
- [29] A.S. Foster, L.N. Kantorovich, A.L. Shluger, *Appl. Phys. A* 72 (2001) S59.
- [30] A.I. Livshits, A.L. Shluger, A.L. Rohl, A.S. Foster, *Phys. Rev. B* 59 (1999) 2436.
- [31] R. Bennewitz, A.S. Foster, L.N. Kantorovich, M. Bammerlin, C. Loppacher, S. Schar, M. Guggisberg, E. Meyer, A.L. Shluger, *Phys. Rev. B* 62 (2000) 2074.
- [32] L.N. Kantorovich, A.I. Livshits, A.M. Stoneham, *J. Phys.: Condens. Mat.* 12 (2000) 795.
- [33] L.N. Kantorovich, A.S. Foster, A.L. Shluger, A.M. Stoneham, *Surf. Sci.* 445 (2000) 283.
- [34] C. Argento, R.H. French, *J. Appl. Phys.* 80 (1996) 6081.
- [35] D.H. Gay, A.L. Rohl, *J. Chem. Soc., Faraday Trans.* 91 (1995) 925.
- [36] A.S. Foster, A.L. Rohl, A.L. Shluger, *Appl. Phys. A* 72 (2001) S31.
- [37] A. Pavese, M. Catti, S.C. Parker, A. Wall, *Phys. Chem. Miner.* 23 (1996) 89.
- [38] A.L. Shluger, A.L. Rohl, D.H. Gay, R.T. Williams, *J. Phys.: Condens. Mat.* 6 (1994) 1825.
- [39] N. Sasaki, M. Tsukada, R. Tamura, K. Abe, N. Sato, *Appl. Phys. A* 66 (1998) S287.
- [40] N. Sasaki, M. Tsukada, *Appl. Surf. Sci.* 140 (1999) 339.
- [41] N. Sasaki, M. Tsukada, *Appl. Phys. A* 72 (2001) S39.
- [42] N.A. Burnham, R.J. Colton, H.M. Pollock, *Nanotechnology* 4 (1993) 64.
- [43] F. Ohnesorge, G. Binnig, *Science* 260 (1993) 1451.
- [44] H. Shindo, H. Nozoye, *Surf. Sci.* 287–288 (1993) 1030.
- [45] S.L.S. Stipp, *Geochem. Cosmochem. Acta* 63 (1999) 3121.
- [46] G. Kresse, J. Furthmuller, *Phys. Rev. B* 54 (1996) 11169.
- [47] G. Kresse, J. Furthmuller, *Comp. Mater. Sci.* 6 (1996) 15.
- [48] J.P. Perdew, J.A. Chevary, S.H. Vosko, K.A. Jackson, M.R. Pederson, D.J. Singh, C. Fiolhais, *Phys. Rev. B* 46 (1992) 6671.
- [49] D. Vanderbilt, *Phys. Rev. B* 41 (1990) 7892.
- [50] G. Kresse, J. Hafner, *J. Phys.: Condens. Mat.* 6 (1994) 8245.